

EDITORIAL

Bioactive Surface Functionalization

K. G. Neoh, *J. Appl. Polym. Sci.* 2014, DOI: [10.1002/app.40607](https://doi.org/10.1002/app.40607)

REVIEWS

Orthogonal surface functionalization through bioactive vapor-based polymer coatings

X. Deng and J. Lahann, *J. Appl. Polym. Sci.* 2014, DOI: [10.1002/app.40315](https://doi.org/10.1002/app.40315)

Surface modifying oligomers used to functionalize polymeric surfaces: Consideration of blood contact applications

M. L. Lopez-Donaire and J. P. Santerre, *J. Appl. Polym. Sci.* 2014, DOI: [10.1002/app.40328](https://doi.org/10.1002/app.40328)

Block copolymers for protein ordering

J. Malmström and J. Travas-Sejdic, *J. Appl. Polym. Sci.* 2014, DOI: [10.1002/app.40360](https://doi.org/10.1002/app.40360)

RESEARCH ARTICLES

MS-monitored conjugation of poly(ethylene glycol) monomethacrylate to RGD peptides

O. I. Bol'shakov and E. O. Akala, *J. Appl. Polym. Sci.* 2014, DOI: [10.1002/app.40385](https://doi.org/10.1002/app.40385)

Synthesis and characterization of surface-grafted poly(*N*-isopropylacrylamide) and poly(carboxylic acid)—Iron particles via atom transfer radical polymerization for biomedical applications

J. Sutrisno, A. Fuchs and C. Evrensel, *J. Appl. Polym. Sci.* 2014, DOI: [10.1002/app.40176](https://doi.org/10.1002/app.40176)

Deposition of nonfouling plasma polymers to a thermoplastic silicone elastomer for microfluidic and biomedical applications

P. Gross-Kosche, S. P. Low, R. Guo, D. A. Steele and A. Michelmore, *J. Appl. Polym. Sci.* 2014, DOI: [10.1002/app.40500](https://doi.org/10.1002/app.40500)

Regeneration effect of visible light-curing furfuryl alginate compound by release of epidermal growth factor for wound healing application

Y. Heo, H.-J. Lee, E.-H. Kim, M.-K. Kim, Y. Ito and T.-I. Son, *J. Appl. Polym. Sci.* 2014, DOI: [10.1002/app.40113](https://doi.org/10.1002/app.40113)

Bioactive agarose carbon-nanotube composites are capable of manipulating brain-implant interface

D. Y. Lewitus, K. L. Smith, J. Landers, A. V. Neimark and J. Kohn, *J. Appl. Polym. Sci.* 2014, DOI: [10.1002/app.40297](https://doi.org/10.1002/app.40297)

Preparation and characterization of 2-methacryloyloxyethyl phosphorylcholine (MPC) polymer nanofibers prepared via electrospinning for biomedical materials

T. Maeda, K. Hagiwara, S. Yoshida, T. Hasebe and A. Hotta, *J. Appl. Polym. Sci.* 2014, DOI: [10.1002/app.40606](https://doi.org/10.1002/app.40606)

Nanostructured polystyrene films engineered by plasma processes: Surface characterization and stem cell interaction

S. Mattioli, S. Martino, F. D'Angelo, C. Emiliani, J. M. Kenny and I. Armentano, *J. Appl. Polym. Sci.* 2014, DOI: [10.1002/app.40427](https://doi.org/10.1002/app.40427)

Microtextured polystyrene surfaces for three-dimensional cell culture made by a simple solvent treatment method

M. E. DeRosa, Y. Hong, R. A. Faris and H. Rao, *J. Appl. Polym. Sci.* 2014, DOI: [10.1002/app.40181](https://doi.org/10.1002/app.40181)

Elastic biodegradable starch/ethylene-co-vinyl alcohol fibre-mesh scaffolds for tissue engineering applications

M. A. Susano, I. B. Leonor, R. L. Reis and H. S. Azevedo, *J. Appl. Polym. Sci.* 2014, DOI: [10.1002/app.40504](https://doi.org/10.1002/app.40504)

Fibroblast viability and inhibitory activity against *Pseudomonas aeruginosa* in lactic acid-grafted chitosan hydrogels

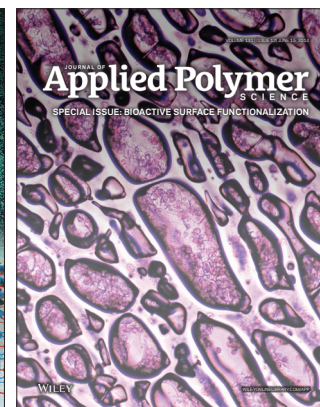
A. Espadín, N. Vázquez, A. Tecante, L. Tamay de Dios, M. Gimeno, C. Velasquillo and K. Shirai, *J. Appl. Polym. Sci.* 2014, DOI: [10.1002/app.40252](https://doi.org/10.1002/app.40252)

Surface activity of pepsin-solubilized collagen acylated by lauroyl chloride along with succinic anhydride

C. Li, W. Liu, L. Duan, Z. Tian and G. Li, *J. Appl. Polym. Sci.* 2014, DOI: [10.1002/app.40174](https://doi.org/10.1002/app.40174)

Collagen immobilized PET-g-PVA fiber prepared by electron beam co-irradiation

G. Dai, H. Xiao, S. Zhu and M. Shi, *J. Appl. Polym. Sci.* 2014, DOI: [10.1002/app.40597](https://doi.org/10.1002/app.40597)



Elastic Biodegradable Starch/Ethylene-co-Vinyl Alcohol Fibre-Mesh Scaffolds for Tissue Engineering Applications

Maria A. Susano,^{1,2} Isabel B. Leonor,^{1,2} Rui L. Reis,^{1,2} Helena S. Azevedo^{1,2}

¹3B's Research Group—Biomaterials, Biodegradables, and Biomimetics, University of Minho, Headquarters of the European Institute of Excellence on Tissue Engineering and Regenerative Medicine, AvePark, 4806-909 Taipas, Guimarães, Portugal

²ICVS/3Bs—PT Government Associate Laboratory, Braga/Guimarães, Portugal

Correspondence to: H. S. Azevedo (E-mail: hazevedo@dep.uminho.pt or h.azevedo@qmul.ac.uk)

ABSTRACT: The fabrication of a biomaterial scaffold, with adequate physical and structural properties for tissue engineering applications, is reported. A blend of starch with ethylene-vinyl alcohol (50/50 w/w, SEVA-C) is used to produce 3D fibre-mesh scaffolds by wet-spinning. The scaffolds are characterized in terms of morphology, porosity, interconnectivity, and pore size, using scanning electron microscopy (SEM) and microcomputed tomography (μ CT). The degradation behavior, as well as the mechanical properties of the scaffolds, is investigated in presence of alpha-amylase enzyme at physiological concentration. Scaffolds with porosities ranging from 43 to 52%, interconnectivity of \sim 70.5% and pore size between 118 and 159 μ m, can be fabricated using the proposed methodology. The scaffolds exhibit an elastic behavior in the wet state with a compressive modulus of 7.96 ± 0.32 MPa. Degradation studies show that SEVA-C scaffolds are susceptible to enzymatic degradation by alpha-amylase, confirmed by the increase of weight loss (40% of weight loss after 12 weeks) and presence of degradation products (reducing sugars) in solution. The diameter of SEVA-C scaffolds decreases with degradation time, increasing the overall porosity, interconnectivity and pore size. *In vitro* cell studies with human osteosarcoma cell line (SaOs-2) showed a nontoxic and cytocompatible behavior of the developed fibre mesh scaffolds. The positive cellular response, together with structural and degradable properties, suggests that 3D SEVA-C fibre-meshes may be good candidates as tissue engineering scaffolds. © 2014 Wiley Periodicals, Inc. *J. Appl. Polym. Sci.* **2014**, *131*, 40504.

KEYWORDS: biodegradable; biomaterials; porous materials; mechanical properties; elastomers

Received 22 October 2013; accepted 23 January 2014

DOI: 10.1002/app.40504

INTRODUCTION

Tissue engineering often makes use of biodegradable scaffolds to guide and promote controlled cellular growth and differentiation in order to generate new tissue. Over the past decades, a variety of scaffolds, made of natural¹ and synthetic^{2,3} polymer-based materials and fabricated by different methods,^{4–7} have been investigated and significant research has been carried out studying the effects of scaffold structural and mechanical properties on tissue formation. Within different tissues, elasticity spans almost three orders of magnitude across brain, fat, muscle, cartilage, and bone.⁸ Elasticity is one intrinsic physical property that is well controlled in many tissues and it is well recognized that cells sense the elasticity of their microenvironments. Therefore, major efforts have been taken to develop elastomeric biomaterials that mimic the elastic behavior of native tissues. Elastomeric biomaterials include chemically crosslinked (silicones, polyolefin and polydiene, poly(polyol sebacate, *cis*-poly(isoprene)) and physically crosslinked (polyurethanes, styrene-based rubbers, polyesters, and copolyesters) elastomers.⁹ Each type of material has its advantages

and disadvantages, in terms of biocompatibility, biodegradability, and mechanical properties. A recent review on the use of elastomeric biomaterials for tissue engineering revealed that ideal elastomeric materials with optimal properties are still not available for clinical applications.⁹

In the recapitulation of cellular microenvironments, scaffolds may play an important role in providing a platform to influence the perception and response of cells to substrate mechanics. In the last years, several studies have demonstrated that the function of cells, in particular stem cells, is affected by collective physical properties (elasticity, topography, and geometry) of materials.^{8,10–12} It is believed that matrix stiffness may regulate cell function by altering cell shape, resulting in cytoskeletal rearrangements and altered signalling. The results suggest the possibility of optimizing matrix elasticity to control cell behavior and foster regeneration.

Our group has reported the preparation of fibres by wet-spinning using a blend of starch with poly(ethylene-vinyl alcohol) copolymer (SEVA-C)¹³ and shown that the obtained wet

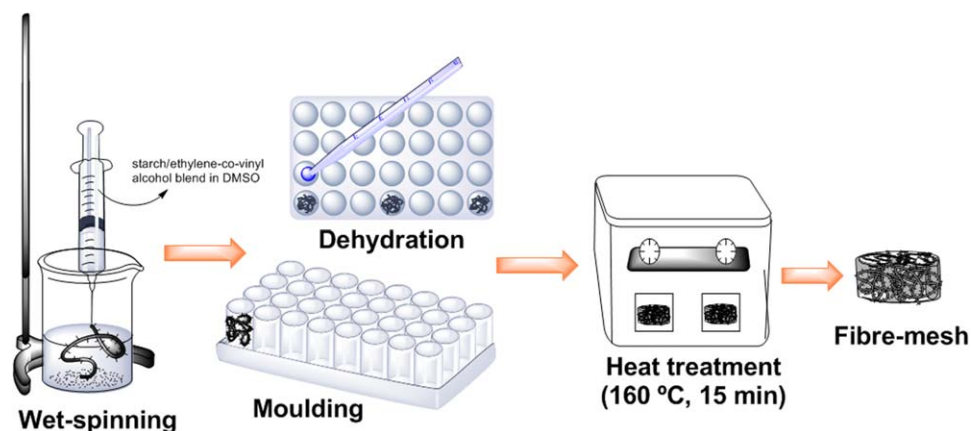


Figure 1. Schematic illustration of the setup for the production of the fibre-mesh scaffolds using wet-spinning technique. [Color figure can be viewed in the online issue, which is available at wileyonlinelibrary.com.]

spun fibres presented some interesting features when compared with melt spun fibres using the same polymeric blend.¹⁴ Thinner and much stiffer fibres can be produced and their rough surface may favour cell adhesion. In this article, the fabrication of 3D fibre-mesh scaffolds using the SEVA-C blend and a nondesigned-controlled technique is described. Their structural, mechanical and degradation characteristics are reported as well as their ability to support cell survival and proliferation.

EXPERIMENTAL

Fabrication of 3D Fibre-Mesh Scaffolds

The scaffolds investigated in this study were fabricated by wet-spinning technique (Figure 1) and using a commercial blend of starch with poly-(ethylene-vinyl alcohol) copolymer (SEVA-C, 50/50 wt%) provided by Novamont (Mater Bi 1128RR, Novara,

Italy). SEVA-C granules were dissolved in dimethyl sulfoxide (DMSO, Riedel-de Haën). The obtained polymer solution (20%, w/v) was loaded into a syringe (12.5-mm diameter, 25-G needle) which was placed in a programmable syringe pump (World Precision Instruments, UK). The polymer solution (0.5 mL) was injected at controlled rate (0.2 mL h^{-1}) directly into a water bath to allow the formation of the fibres [Figure 2(a)]. The fibres were washed several times with distilled water to remove residual DMSO. To ensure reproducibility, fibre-mesh scaffolds were prepared by placing a predetermined volume of fibres in a well of a 48-well cell culture plate. The fibres were dehydrated with increasing concentrations of ethanol (50, 60, 70, 80, 85, 90, 95, and 100%) and then allowed to dry at room temperature. To ensure the bonding between the fibres, the scaffolds were put in the oven for 15 min at 160°C , as shown in

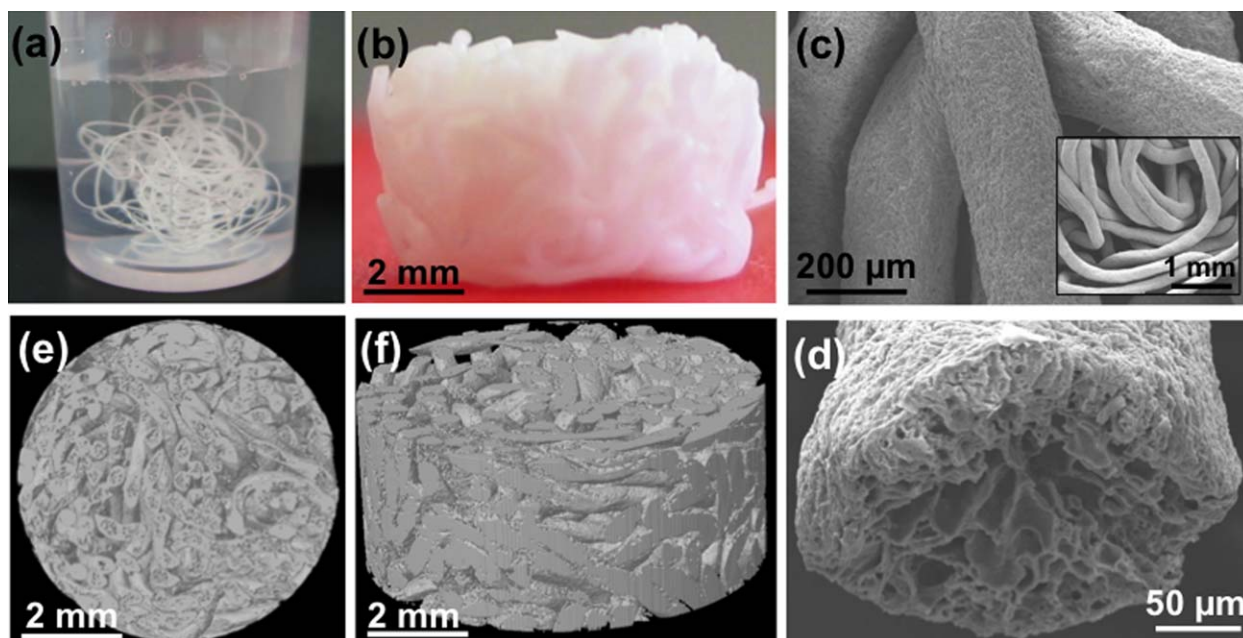


Figure 2. SEVA-C fibres after processing by wet-spinning (a) and after moulding into a 3D structure (b). SEM images of SEVA-C fibre mesh scaffolds (c) and fibre cross-section (d). Inset in (c) is lower magnification of SEM image. The 2D (e) and 3D (f) visualizations obtained by μCT analysis. [Color figure can be viewed in the online issue, which is available at wileyonlinelibrary.com.]

Figure 1. For cell culture studies, the scaffolds were sterilized by ethylene oxide, with a cycle time of 14 h at a working temperature of 45°C and a chamber pressure of 50 kPa, conditions previously optimized for the SEVA-C blend.¹⁵

Morphological and Mechanical Characterization of Fibre-Mesh Scaffolds

Scanning Electron Microscopy (SEM). To observe the structure and morphology of the fibre-mesh scaffolds, the samples were mounted onto aluminium stubs with a carbon tape and gold sputter-coated (Fisons Instruments, Sputter Coater SC502, UK). Microphotographs at the surface were collected with a Leica Cambridge S-360 model (Cambridge, UK) scanning electron microscope. The fibre thickness was estimated by measuring the thickness of individual fibres obtained in the SEM images.

Microcomputed Tomography (μ CT). To assess the morphometric parameters (porosity, interconnectivity, and pore size) of the scaffolds, the specimens were scanned in triplicate using a high-resolution μ CT system (Skyscan 1072, Skyscan, Kontich, Belgium). The X-ray scans were acquired in high-resolution mode of 6.59 μ m and an exposure time of 2.1 s. The energy parameters defined in the scanner were 69 keV with a current of 144 μ A. Approximately 400 projections were acquired over a rotation range of 180° with a rotation step of 0.45°. Datasets were reconstructed using standardized cone-beam reconstruction software (NRecon v1.4.3, SkyScan). The output format for each scaffold was 400 serial bitmap images with 1024 \times 1024 pixels. Representative dataset of 200 slides were segmented into binary images with a dynamic threshold of 37–120 (grey values). These data sets were used for morphometric analysis (CT Analyser v1.5.1.5, SkyScan) and to build the 3D virtual models (ANT 3D creator v2.4, SkyScan). The 3D virtual models of representative regions in the bulk of the scaffolds were created, visualized and registered using both images processing software (CT Analyser and ANT 3-D creator).

Mechanical Testing. Compression tests were carried out to evaluate mechanical behavior of the scaffolds in the dry and wet state (scaffolds immersed in PBS for 24 h). Seven specimens with height \sim 3 mm and diameter \sim 7 mm were tested for each condition. They were tested using uniaxial testing system (Instron 5540 Universal Machine, USA) with a load cell of 1 kN. Compression testing was carried out at a crosshead speed of 2 mm min⁻¹, until obtaining a maximum reduction in samples height of 60%. The compressive modulus was determined in the most linear region (strain < 1%) of the stress–strain graph.

Scaffold Degradation

The degradation of the scaffolds was assessed in absence and presence of α -amylase enzyme to study its effect on starch hydrolysis. Preweighed fibre-mesh scaffolds (previously dried under vacuum at 60°C for 48 h) were individually immersed in 2 mL of phosphate-buffered saline (PBS, 0.01 M, pH 7.4) solution containing 160 U L⁻¹ α -amylase (EC 3.2.1.1, from *Bacillus* sp., Sigma) and incubated for 1, 4, 8, and 12 weeks at 37°C. Sodium azide (0.02%) was added to the buffer solution to prevent microbial growth. The degradation solutions were changed weekly. A control, in PBS only, was also performed and five samples were analyzed for each condition. After each

degradation period, the samples were removed from the solution and placed between two filter papers, to remove excess of liquid, immediately weighed, washed several times with distilled water and placed in the vacuum oven at 60°C for 48 h in order to determine water uptake and weight loss. The degraded scaffolds were also analyzed by SEM, μ CT and the mechanical properties were evaluated in the wet state, as described above. Degradation solutions (collected every week) were analyzed to determine the concentration of reducing sugars released into the solution as result of starch hydrolysis. The determination of reducing sugars in solution was based on the dinitrosalicylic acid (DNS) method.¹⁶ Absorbance was read at 540 nm in a microplate reader (Synergy HT, BIO-TEK Instruments, USA) using a standard curve of glucose. The concentration of reducing sugars at each degradation time was calculated as cumulative values obtained from the weekly determinations.

Cell Culture Studies

To investigate if the SEVA-C scaffolds can support cell viability and proliferation, an established human osteosarcoma cell line (SaOs-2) obtained from European Collection of Cell Cultures (ECACC, UK) was used. Cells cultured onto tissue culture polystyrene (TCPS) with standard culture medium were used as a negative control. Prior cell seeding, cells were cultured in DMEM (Dulbecco's-Modified Eagle's Medium, Sigma, Germany) supplemented with 10% fetal bovine serum (Gibco, UK), 1% antibiotic-antimycotic (Gibco, UK) solution containing 10,000 U mL⁻¹ penicillin G sodium, 10,000 μ g mL⁻¹ streptomycin sulfate and 25 μ g mL⁻¹ amphotericin B as Fungizone® in 0.85% saline in a humidified atmosphere with 5% CO₂ and at 37°C. When confluence was reached, cells were trypsinized (0.25% trypsin/EDTA solution, Sigma Chemical, USA) from the culture flask and diluted to achieve a cellular concentration of 26,000 cells mL⁻¹. Afterwards, 50 μ L of a cell suspension was dropped onto the 3D scaffolds, individually placed in each well of a 48-well cell culture plate, and incubated for 4 h in 5% CO₂ incubator at 37°C. Subsequently, 500 μ L of DMEM were added to the wells and further incubated for 1, 3, 7, and 14 days in the same conditions. The culture medium was changed every 2 days. Viability of cells was assessed by the MTS assay and cell proliferation evaluated by DNA quantification, as described below.

Cell Viability. Cell viability was determined by means of a standard MTS (3-(4,5-dimethylthiazol-2-yl)-5-(3-carboxymethoxyphenyl)-2-(4-sulfophenyl)-2H-tetrazolium) assay. The MTS test was performed according to the manufacturer's instructions (CellTiter 96 One Solution Proliferation Assay Kit, Promega, USA). Briefly, the cell cultured scaffolds were treated with 200 μ L of MTS reagent solution in serum-free DMEM without phenol red (5 : 1 ratio) and incubated for 3 h at 37°C in a humidified environment containing 5% of CO₂. About 100 μ L of medium from each well were transferred to a 96-well plate and the absorbance at 490 nm was determined in the microplate reader (Synergy HT, BioTek Instruments, USA). The absorbance of each sample from three independent assays was measured in triplicate. Unseeded scaffolds were used as controls.

Cell Proliferation. Cell proliferation was evaluated by quantifying the DNA amount of the cells in the scaffolds at different time points using PicoGreen® DNA quantification assay (Molecular Probes, USA). The DNA of cultured cells was extracted by osmotic lysis and thermal shock. Cell cultured scaffolds were collected, washed twice with sterile PBS (Sigma, USA) solution and transferred into 1.5 mL tubes containing 1 mL of ultra-pure water. Scaffolds, with or without cells, were stored at -80°C . Samples were thawed and the supernatant was collected for DNA quantification following the manufacturer's instructions. The fluorescence was measured (485 nm excitation and 528 nm emission) in a microplate reader (Synergy HT, Bio-Tek Instruments, USA). The DNA amounts were calculated from a calibration curve of DNA standards. Each sample was analyzed in triplicate.

Statistical Analysis

All data are given as mean \pm standard deviation (SD) for $n = 5$ (degradation), $n = 7$ (mechanical testing), and $n = 3$ (μCT and *in vitro* cell culture experiments). Normality test, Shapiro–Wilk, was performed to insure data set is well-modelled by a normal distribution. A statistical hypothesis test using a Student's *t* distribution (two samples *t* test) was used to identify differences in the results. The data analyses were performed with OriginPro software (version 8) and differences were considered significant at $P < 0.05$.

RESULTS AND DISCUSSION

Morphological Characterization

In scaffold-based tissue engineering, scaffold architectural features should be designed to allow the diffusion of nutrients and cell migration and thus promoting optimal tissue ingrowth *in vivo*. Some of these important architectural characteristics include porosity, pore size and interconnectivity. In the present study, SEVA-C fibres were produced by wet-spinning [Figure 2(a)] and moulded into a cylindrical shape [Figure 2(b)]. To maintain the fibres within the mesh when immersed in aqueous solutions, the obtained scaffolds were further submitted to a heat treatment for binding the fibres. μCT and SEM were used to assess the relevant morphometric parameters of the scaffolds. SEM images show fibres with an average thickness of $215\ \mu\text{m}$ and rough surface [Figure 2(c,d)] which may provide favourable anchorage sites for cell attachment. Representative 3D images of the scaffolds by μCT reveal a fibre mesh structure with a random distribution of the fibres within the mesh and a good level of interconnectivity [Figure 2(e,f)]. This type of scaffold provides a highly permeable, interconnected structure with a large surface area. The SEVA-C scaffolds have a pore volume fraction of $47.3\% \pm 5.16\%$ with an interconnectivity of $70.5\% \pm 4.12\%$, as determined by μCT analysis. Porosity is a key property since it determines cell seeding efficiency, diffusion and the mechanical strength of the scaffold. When molecular transport is hampered, due to poor diffusion, cell-scaffold constructs exhibit peripheral cellular growth while the interior of the construct undergoes necrosis.¹⁷ In addition, high porosity (up 90%) is recommended to enhance cellular attachment and neo-tissue ingrowth under *in vivo* conditions.^{2,18,19} Although the values for porosity might be considered low when compared with the ones

reported as optimal for bone regeneration, other factors should be considered when designing the scaffold porosity, like the degradation rate of the scaffold and the intended application. Porosity is expected to increase with degradation¹⁹ and high porosity may constrain the mechanical strength⁶ of the scaffold which may be critical for the regeneration of load-bearing tissues such as bone.

The functionality of tissue engineering scaffolds is also related with the size of the pores. An exact pore size cannot be suggested as a general guide for optimal tissue outcomes, due to the specificity of each tissue to be engineered. Relatively larger pores favour direct tissue regeneration since they allow vascularization and high oxygenation. Specifically, in bone tissue engineering, the consensus seems to be that the optimal pore size for bone ingrowth is $100\text{--}400\ \mu\text{m}$.^{20–22} However, more recently, studies have shown that 3D structures containing microporosity ($<10\ \mu\text{m}$) as well as macroporosity ($>50\ \mu\text{m}$), a multiscale porosity, can further promote bone ingrowth.^{23,24} Conversely, scaffolds that contained only macroporosity, and no microporosity, had no bone ingrowth.²⁴ The developed scaffold shows a mean pore size of $138.9\ \mu\text{m} \pm 20.37\ \mu\text{m}$ and pore distribution with sizes between 30 and $280\ \mu\text{m}$ (data not shown), in the range of the optimal pore size for bone ingrowth and simultaneously for a fast osseointegration. The distribution of fibres within the mesh influences the pore size, which can be controlled by the amount of fibres used for the scaffold production and also by the degree of compaction of the fibres.

Most polymeric fibres described in the literature and obtained from other processing techniques exhibit a very dense core.^{14,25,26} In contrast, the SEVA-C fibres show an internal porous structure, as observed in the SEM micrographs of the fibre cross-section [Figure 2(d)]. We anticipate that this internal porosity may be a beneficial attribute for the incorporation and sustained release of differentiation agents relevant in tissue engineering applications.

The nondesigned-controlled technique used in this study allows attaining some control over the 3D architecture, in terms of porosity and pore size, by altering some processing parameters, such as fibre diameter and volume of fibres. However, one has to consider that there is a compromise between porosity and mechanical behaviour. An increase in the void volume results in a reduction in the mechanical strength of the scaffold, which can be critical for tissue regeneration. On the other hand, a highly porous scaffold may not have interconnected pores, thus lowering the diffusion efficiency.²⁷ Studies performed by Suh et al. showed superior cell attachment and proliferation of chondrocytes in scaffolds with high interconnectivity and equal porosity.²⁸ Lu et al. also reported the importance of interconnectivity for bone ingrowth.²⁹ Thus, a high interconnected structure, such as the one proposed herein, is essential to allow the diffusion of culture medium, metabolic waste, and oxygen, and to facilitate the infiltration and proliferation of cells.³⁰

Mechanical Characterization

The magnitudes of mechanical stresses that tissues may be subjected *in vivo* can be quite large, and few engineered tissue constructs possess the properties to withstand such stresses at the


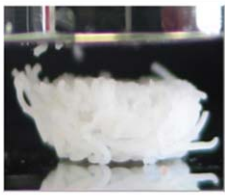
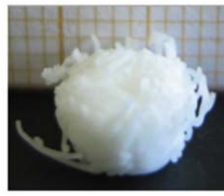

Initial	Immediately after compression	2 h after compression	24 h after compression
			
Height: 3.9 mm Ø = 7.8 mm	Height: 1.6 mm Ø = 9.2 mm	Height: 2.9 mm Ø = 8.2 mm	Height: 3.7 mm Ø = 7.9 mm

Figure 3. Scaffold dimensions in terms of height and diameter (\varnothing) before and after compression test (load cell of 1 kN; crosshead speed 2 mm min⁻¹; 60% strain). [Color figure can be viewed in the online issue, which is available at wileyonlinelibrary.com.]

time of implantation. The challenge is not only matching a single mechanical parameter of the tissue to be engineered, such as modulus or strength, but one needs to consider that most tissues possess complex viscoelastic, non linear, and anisotropic mechanical properties that may vary with age, site, and some other factors. The maintenance of the scaffold structural integrity is important for achieving stable biomechanical conditions at the host site.³¹ Additionally, in the case of load-bearing tissue, such as cartilage and bone, the scaffold matrix must provide sufficient mechanical support to withstand *in vivo* stress and loading.⁶ There are a couple of important considerations regarding the scaffold properties for hard tissues. As pointed by Cordell et al.,³² one must consider that the stiffness of the scaffolds would increase with tissue ingrowth, especially in slowly degrading materials. Although the mechanical properties of bone depends on its structure and orientation, the values of compressive modulus of normal wet human cancellous bone reported in the literature vary between 12 and 900 MPa.³³ While many studies report the mechanical properties of scaffolds in the dry state, assessing their mechanical behavior in the hydrated state is physiologically more relevant. As expected, the results of mechanical testing demonstrate that the values of compressive modulus for SEVA-C scaffolds are clearly different in the dry and wet state. In the dry state, the SEVA-C scaffolds exhibited a compressive modulus (E) of 24.31 ± 2.91 MPa, while in the wet state the compressive modulus is reduced to 7.96 ± 0.32 MPa. One explanation in the decrease of the modulus after immersion in PBS can be attributed to the plasticization effect due to the absorbed water. SEVA-C is a very hydrophilic material and after being in contact with aqueous solutions absorbs water, becoming more flexible that result in a decrease of compressive modulus. Although these values are considered below the ones required for bone applications, SEVA-C scaffolds present higher compressive modulus than other fibre-mesh scaffolds obtained from blends of starch with biodegradable polyesters (polycaprolactone and poly(lactic acid)).³⁴ The mechanical properties of the developed scaffolds can be enhanced by coating the SEVA-C fibres with calcium-phosphate layer. Interestingly, the mechanical characterization of SEVA-C scaffolds in the wet state showed that after compression, SEVA-C fibre mesh scaffolds present an elastic behavior since they recover almost completely their original dimensions within 24 h (Figure 3). This indicates a remarkable ability to withstand firm thumb

pressure without permanent deformation. On the contrary, in the dry state, the deformation consequence of compression load is permanent. In addition, hydrated SEVA-C scaffolds possess adequate compressive modulus to support their shape without

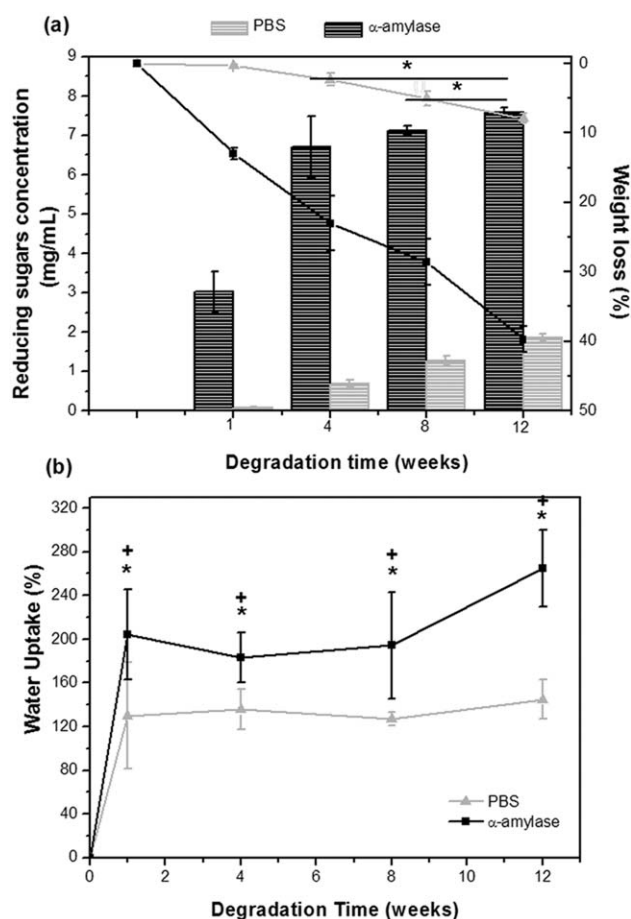


Figure 4. Degradation profile of the SEVA-C fibre-mesh scaffolds measured in terms of (a) weight loss (line) and reducing sugar concentration (bar) and (b) water uptake in PBS solution (pH 7.4, 37°C) and in presence of α -amylase. A single asterisk (*) indicates a significant difference ($P < 0.05$) for the same condition at different time points. A plus (+) indicates a significant difference ($P < 0.05$) between conditions for the same time point.

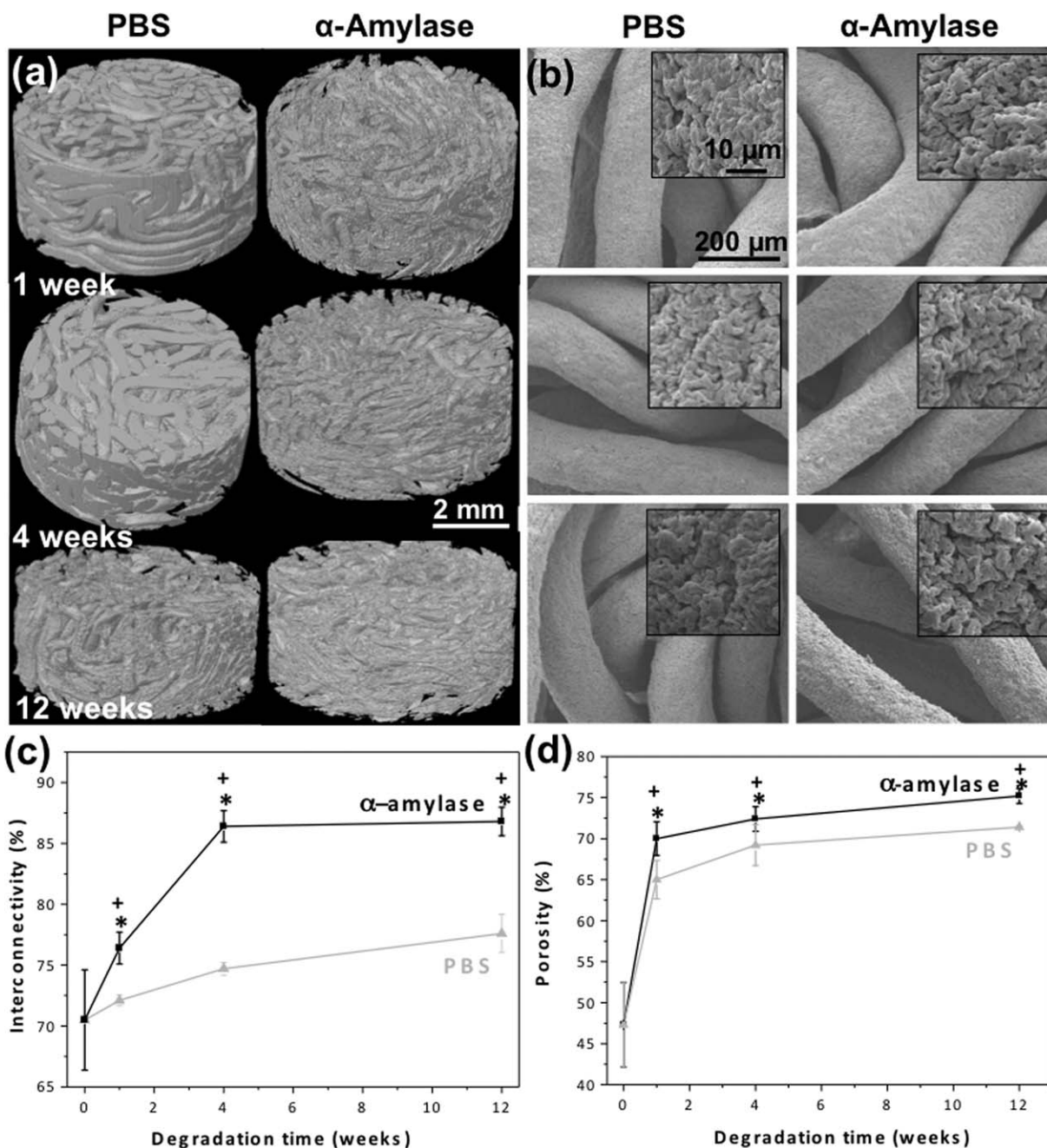


Figure 5. μ CT (a) and SEM (b) images of SEVA-C fibre mesh scaffolds after 1, 4, and 12 weeks of degradation in PBS and α -amylase solutions. Insets in (b) are magnified images of SEM images. Interconnectivity (c) and porosity (d) of SEVA-C fibre-mesh scaffolds as function of degradation time in PBS solution and in presence of α -amylase (pH 7.4, 37°C). A single asterisk (*) indicates a significant difference ($P < 0.05$) for the same condition at different time points. A plus (+) indicates a significant difference ($P < 0.05$) between conditions for the same time point.

structure collapse and thereby maintaining pore structure in 3D. The elastic behavior of the scaffold represents an important advantage since the scaffolds can be subjected to mechanical stimuli during cell culture without being permanently deformed, as mechanical forces are believed to affect cellular distribution,³⁵ metabolic activity³⁶ and ultimately the mechanical properties of the tissue itself.³⁷ Therefore, the 3D structures proposed herein show a good combination of morphometric parameters and mechanical performance.

Degradation Behavior

Under physiological conditions, biodegradable polymers are mainly degraded by hydrolysis followed by oxidation. There are two different mechanisms for hydrolysis: polymers that are decomposed by enzyme-specific reactions (enzymatically degradable polymers) and polymers that are decomposed by contact with water or serum. α -Amylase is a glycosidic hydrolase that acts on the α (1–4) glycosidic bonds of starch molecules reducing its molecular weight, and yielding maltose, glucose

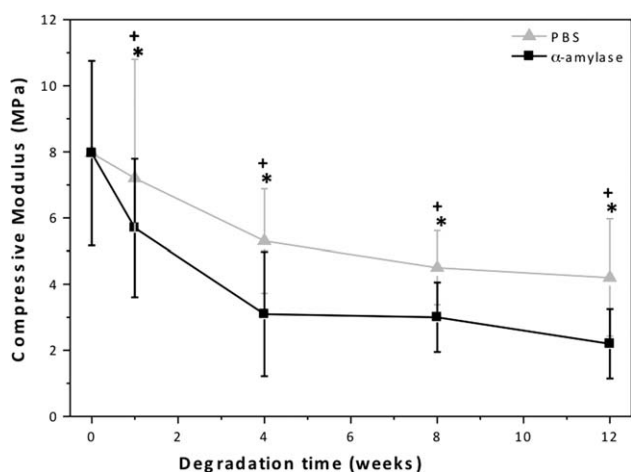


Figure 6. Compressive modulus of SEVA-C fibre-mesh scaffolds in the wet state as function of degradation time in PBS solution and in presence of α -amylase (pH 7.4, 37°C). A single asterisk (*) indicates a significant difference ($P < 0.05$) for the same condition at different time points. A plus (+) indicates a significant difference ($P < 0.05$) between conditions for the same time point.

and other small sugar molecules. In humans, the enzyme occurs in a variety of tissues, but the highest concentrations are in the pancreas and in salivary glands. Low amylase activities are normally detected in the serum (46–244 U L⁻¹) of healthy subjects.³⁸ Having into account the catalytic activity of α -amylase, the degradation behavior of SEVA-C scaffolds was studied in presence of this enzyme at a physiological concentration (160 U L⁻¹). Degradation was assessed by following the scaffold weight loss and water uptake along the time (Figure 4). The concentration of reducing sugars in solution was also determined since it can be used to estimate the degradation of polysaccharide materials. Polysaccharide that are reducing sugars, generally have only one residue that lacks a glycosidic linkage, the so-called reducing end. When consecutively hydrolysis of glycosidic linkages occurs, there is the release of soluble reducing sugars into the solution, which can be quantified.

The scaffolds kept in PBS, devoid of enzymes, showed lower degradation rate (<10% weight loss after 12 weeks of incubation) comparing with ones in amylase solution (~40% weight loss). The low percentage of weight loss in PBS reveals the stability of the scaffolds in buffer solutions. Moreover, the fibre mesh scaffolds had enough mechanical integrity to remain intact throughout the water uptake and degradation study. Previous studies have already demonstrated the biodegradable character of SEVA-C materials³⁹ but these studies were performed on compact samples processed by injection moulding. The presence of starch increases the biodegradability of the blend making it susceptible to enzyme degradation by α -amylase. As the degradation time increases, an accentuated increase in the concentration of sugars in solution is observed confirming the degradation of starch in the scaffold. The concentration of sugars in solution when the scaffold was incubated in the enzyme solution (8 mg mL⁻¹) is about five times higher than the value found in PBS only (1.8 mg mL⁻¹) at 12 weeks. Water uptake

was also investigated along degradation time [Figure 4(b)]. When immersed in PBS, the water up-take is about 120% after 1 week and remains constant with time. The high values of water uptake are related with the hydrophilic nature of the SEVA-C material (presence of —OH groups in starch and EVOH) and also with the high surface area of the fibre mesh scaffold. In the enzymatic solution, higher water uptake was observed in the first week (~200%) which increases gradually with time of degradation. The enhanced permeability of the material over time, caused by enzymatic degradation, leads to increased water absorption.

To assess the effect of degradation on the scaffold 3D structure, μ CT and SEM analyses were performed (Figure 5). Changes in the scaffold structure at the surface level were detected, being more visible after 12 weeks of degradation, where a rougher surface is observed [Figure 5(b)]. The morphological changes, porosity and interconnectivity during degradation were examined by μ CT. The results of the morphological analysis [Figure 5(c,d)] show an increase in the interconnectivity for the scaffolds immersed in the enzymatic solution, about 17%, while for

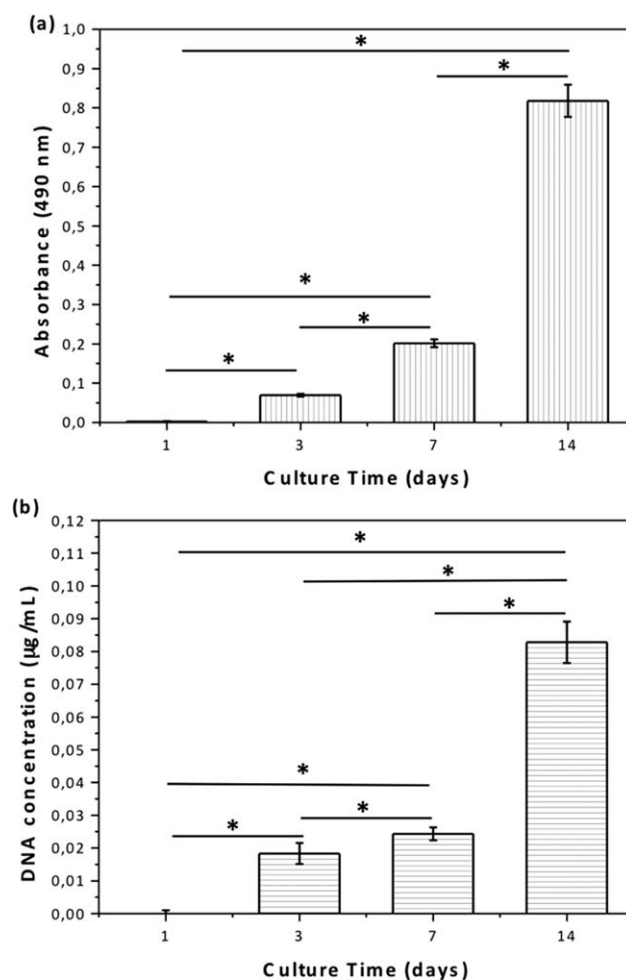


Figure 7. Viability (a) and proliferation (b) of SaOs-2 cells cultured on SEVA-C fibre mesh scaffolds for 1, 3, 7, and 14 days determined by the MTS assay and DNA quantification, respectively. A single asterisk (*) indicates a significant difference ($P < 0.05$) at different time points.

the samples immersed in PBS the increase was not so notorious (~5%). In terms of porosity, a similar trend was observed with an increase in the void volume of the scaffolds with degradation time. The porosities of scaffolds in PBS and enzymatic solution after 12 weeks are 71 and 75%, respectively [Figure 5(d), an increase of almost 30% related with initial porosity]. Surface morphology is also affected during scaffold degradation. The scaffolds immersed in amylase solution present notorious changes on the surface morphology, whereas the scaffolds immersed in PBS did not show evident surface alterations [Figure 5(b)]. After 4 weeks of degradation, there is a noticeable increase on surface roughness, being this observation more pronounced after 12 weeks. Moreover, a decrease in the diameter of the scaffolds was also observed after degradation [Figure 5(a)]. The removal of starch component by enzyme hydrolytic activity leads to the partial matrix collapse⁴⁰ culminating in a reduction of the scaffold size. This is a very important aspect considering that the degradation profile of a scaffold material should leave enough space for new tissue ingrowth.³⁴

Because the mechanical properties affect scaffold functionality, the compressive modulus of the scaffolds was determined along the degradation time. As expected, the scaffold mechanical properties are affected by the scaffold degradation (Figure 6). The decrease in the compressive modulus is associated with increased porosity observed along degradation. The lower values in compressive modulus are more pronounced for the scaffolds immersed in the enzymatic solution, in which a reduction of about 75% was observed after 12 weeks of degradation. For the scaffolds immersed in PBS only, the compressive modulus was ~4 MPa after 12 weeks.

Cellular Viability and Proliferation

To consider the use of the scaffolds in tissue engineering, the biocompatibility of the scaffolds in regards to cell viability and proliferation was evaluated. MTS assay [Figure 7(a)] proved that cells seeded on the scaffolds remain viable, as observed by an increased metabolic activity with culturing time, indicating that the scaffolds did not have any toxic effect on the cells. DNA quantification was also performed to evaluate cell proliferation [Figure 7(b)]. With the progress of culture period, a significant increase in DNA amount was observed, indicating an increase in cell proliferation. Although for initial times (until 7 days) the amount of quantified DNA was lower, the initial *in vitro* performance of scaffold materials is determined by the intrinsic properties of the 3D structure when the first occurring events are related with cell-biomaterial interaction. At later stages, other factors, such as cell to cell contact, are expected to play a significant role. These results indicate that the developed scaffolds may be adequate for the growth of other cell types (stem cells) and future studies will be performed to evaluate cell attachment, proliferation and differentiation of mesenchymal stem cells on these fibre-mesh scaffolds.

CONCLUSIONS

The 3D fibre-mesh scaffolds made of a blend of starch with poly-(ethylene-vinyl alcohol) copolymer were successfully prepared by wet-spinning. The scaffolds showed interesting

properties, including a structure with high porosity and surface area for cell attachment and infiltration; susceptibility to enzymatic degradation (40% of weight loss after 12 weeks) keeping adequate structure for tissue ingrowth; and elastic behavior in the wet state (the scaffolds are able to rapidly recover the initial structure after compression), which represents an additional advantage when compared with existing scaffold materials. Moreover, *in vitro* studies showed that the developed scaffolds support cell viability and proliferation. The positive cellular response, together with structural and degradable properties, suggests that 3D SEVA-C fibre-meshes may be good candidates as tissue engineering scaffolds.

ACKNOWLEDGMENTS

This work was supported by national funds through the Portuguese Foundation for Science and Technology under the scope of the project PTDC/CTM/67560/2006 and by the European Regional Development Fund (ERDF) through the Operational Competitiveness Programme "COMPETE" (FCOMP-01-0124-FEDER-007148). The authors thank Dr Emanuel Fernandes of the 3B's Research Group at the University of Minho for his assistance analyzing the data from mechanical tests.

REFERENCES

1. Mano, J. F.; Silva, G. A.; Azevedo, H. S.; Malafaya, P. B.; Sousa, R. A.; Silva, S. S.; Boesel, L. F.; Oliveira, J. M.; Santos, T. C.; Marques, A. P.; Neves, N. M.; Reis, R. L. J. R. *Soc. Interface* **2007**, *4*, 999.
2. Freed, L. E.; Vunjaknovakovic, G.; Biron, R. J.; Eagles, D. B.; Lesnoy, D. C.; Barlow, S. K.; Langer, R. *Bio-Technology* **1994**, *12*, 689.
3. Martina, M.; Hutmacher, D. W. *Polym. Int.* **2007**, *56*, 145.
4. Weigel, T.; Schinkel, G.; Lendlein, A. *Expert Rev. Med. Dev.* **2006**, *3*, 835.
5. Liu, C.; Xia, Z.; Czernuszka, J. T. *Chem. Eng. Res. Des.* **2007**, *85*, 1051.
6. Hollister, S. J. *Nat. Mater.* **2005**, *4*, 518.
7. Hollister, S. J. *Adv. Mater.* **2009**, *21*, 3330.
8. Engler, A. J.; Sen, S.; Sweeney, H. L.; Discher, D. E. *Cell* **2006**, *126*, 677.
9. Chen, Q. Z.; Liang, S. L.; Thouas, G. A. *Prog. Polym. Sci.* **2013**, *38*, 584.
10. Discher, D. E.; Janmey, P.; Wang, Y. L. *Science* **2005**, *310*, 1139.
11. Thomas, W. E.; Discher, D. E.; Shastri, V. P. *MRS Bull.* **2010**, *35*, 578.
12. Gilbert, P. M.; Havenstrite, K. L.; Magnusson, K. E. G.; Sacco, A.; Leonardi, N. A.; Kraft, P.; Nguyen, N. K.; Thrun, S.; Lutolf, M. P.; Blau, H. M. *Science* **2010**, *329*, 1078.
13. Pashkuleva, I.; Lopez-Perez, P. M.; Azevedo, H. S.; Reis, R. L. *Mater. Sci. Eng. C: Mater. Biol. Appl.* **2010**, *30*, 981.
14. Pavlov, M. P.; Mano, J. F.; Neves, N. M.; Reis, R. L. *Macromol. Biosci.* **2004**, *4*, 776.

15. Reis, R. L.; Mendes, S. C.; Cunha, A. M.; Bevis, M. J. *Polym. Int.* **1997**, *43*, 347.
16. Ghose, T. K. *Pure Appl. Chem.* **1987**, *59*, 257.
17. Ishaug, S. L.; Crane, G. M.; Miller, M. J.; Yasko, A. W.; Yaszemski, M. J.; Mikos, A. G. *J. Biomed. Mater. Res.* **1997**, *36*, 17.
18. Kim, B. S.; Mooney, D. J. *Trends Biotechnol.* **1998**, *16*, 224.
19. Karageorgiou, V.; Kaplan, D. *Biomaterials* **2005**, *26*, 5474.
20. Bobyn, J. D.; Pilliar, R. M.; Cameron, H. U.; Weatherly, G. C. *Clin. Orthopaed. Relat. Res.* **1980**, *150*, 263.
21. Otsuki, B.; Takemoto, M.; Fujibayashi, S.; Neo, M.; Kokubo, T.; Nakamura, T. *Biomaterials* **2006**, *27*, 5892.
22. Mastrogiacomo, M.; Scaglione, S.; Martinetti, R.; Dolcini, L.; Beltrame, F.; Cancedda, R.; Quarto, R. *Biomaterials* **2006**, *27*, 3230.
23. Dellinger, J. G.; Eurell, J. A. C.; Jamison, R. D. *J. Biomed. Mater. Res. A* **2006**, *79A*, 223.
24. Woodard, J. R.; Hildore, A. J.; Lan, S. K.; Park, C. J.; Morgan, A. W.; Eurell, J. A. C.; Clark, S. G.; Wheeler, M. B.; Jamison, R. D.; Johnson, A. J. W. *Biomaterials* **2007**, *28*, 45.
25. Chung, S.; Gamcsik, M. P.; King, M. W. *Biomed. Mater.* **2011**, 045001.
26. Correló, V. M.; A. R. Costa-Pinto, P. Sol, J. A. Covas, M. Bhattacharya, N. M. Neves, R. L. Reis, V. M. *Macromol. Biosci.* **2010**, *10*, 1495.
27. Ho, S. T.; Hutmacher, D. W. *Biomaterials* **2006**, *27*, 1362.
28. Suh, S. W.; Shin, J. Y.; Kim, J. H.; Kim, J. G.; Beak, C. H.; Kim, D. I.; Kim, S. J.; Jeon, S. S.; Choo, I. W. *Asaio J.* **2002**, *48*, 460.
29. Lu, J. X.; Flautre, B.; Anselme, K.; Hardouin, P.; Gallur, A.; Descamps, M.; Thierry, B. *J. Mater. Sci. Mater. Med.* **1999**, *10*, 111.
30. O'Brien, F. J.; Harley, B. A.; Yannas, I. V.; Gibson, L. J. *Biomaterials* **2005**, *26*, 433.
31. Malafaya, P. B.; Santos, T. C.; van Griensven, M.; Reis, R. L. *Biomaterials* **2008**, *29*, 3914.
32. Cordell, J. M.; Vogl, M. L.; Johnson, A. J. W. *J. Mech. Behav. Biomed. Mater.* **2009**, *2*, 560.
33. Athanasiou, K. A.; Zhu, C. F.; Lanctot, D. R.; Agrawal, C. M.; Wang, X. *Tissue Eng.* **2000**, *6*, 361.
34. Gomes, M. E.; Azevedo, H. S.; Moreira, A. R.; Ella, V.; Kellomaki, M.; Reis, R. L. *J. Tissue Eng. Regen. Med.* **2008**, *2*, 243.
35. Egli, P. S.; Hunziker, E. B.; Schenk, R. K. *Anatom. Rec.* **1988**, *222*, 217.
36. Vanwanseele, B.; Lucchinetti, E.; Stussi, E. *Osteoarthritis Cartilage* **2002**, *10*, 408.
37. Swann, A. C.; Seedhom, B. B. *Br. J. Rheumatol.* **1993**, *32*, 16.
38. Isenman, L.; Liebowand, C.; Rothman, S. *Am. J. Physiol. Endocrinol. Metab.* **1999**, *276*, E223.
39. Azevedo, H. S.; Gama, F. M.; Reis, R. L. *Biomacromolecules* **2003**, *4*, 1703.
40. Azevedo, H. S.; Reis, R. L. *Acta Biomater.* **2009**, *5*, 3021.